Research Article Vol. 57, No. 15 / 20 May 2018 / Applied Optics 4283

applied optics

Stokes polarimeter performance: general noise model and analysis

Nathan Hagen* and Yukitoshi Otani

Utsunomiya University, Department of Optical Engineering, Center for Optical Research and Engineering, 7-1-2 Yoto, Utsunomiya, Tochigi 321-0954, Japan
**Corresponding author: nh@hagenlab.org*

Received 17 November 2017; accepted 16 April 2018; posted 20 April 2018 (Doc. ID 313742); published 18 May 2018

We calculate the photometric Stokes parameter covariance matrices and SNRs estimated by polarimeters exposed to general noise distributions, such as mixed Poisson–Gaussian (PG) noise. The measurement model includes the effects of optical losses and detector quantum efficiency, enabling quantitative comparison of instruments that have different photometric efficiencies. We demonstrate this capability by comparing the performance of many common polarimeter configurations, including diattenuator-based systems, such as Azzam's four-detector polarimeter [Opt. Lett. 10, 309 (1985)] and Kudenov's stacked photovoltaic polarimeter [Opt. Express 24, 14737 (2016)]. Working with the full covariance matrix under mixed PG noise, we also show that instruments optimized under assumptions of Gaussian noise simultaneously exhibit optimal behavior under Poisson noise.

OCIS codes: (260.5430) Polarization; (280.0280) Remote sensing and sensors; (230.5440) Polarization-selective devices; (030.4280) Noise in imaging systems.

https://doi.org/10.1364/AO.57.004283

1. INTRODUCTION

A number of researchers have worked on characterizing and optimizing the performance of Stokes polarimeters [1–4]. Whereas the predominant performance metric has been the condition number of the polarimetric measurement matrix, or the equally weighted variance (EWV) of the Stokes parameters, more recent research has included the use of parameter variances and covariances. Most analyses have assumed independent identically distributed Gaussian noise (IG). Most modern systems, however, operate in the shot-noise-limited noise regime, and so a more appropriate model is Poisson-distributed noise (PP, for "pure Poisson"). To incorporate both regimes, we form a mixed Poisson–Gaussian (PG) noise model, which can be taken as Gaussian or Poisson in the limit of small or large detector noise. Thus, the three important noise regimes for optical instruments can be written as IG, PG, or PP, in order of increasing shot noise.

The focus on condition number and EWV as performance metrics obscures important differences between systems, such as detection efficiency, and ignores unequal variance values and correlations among the various Stokes parameter estimates. Our analysis in the following fills in each of these three gaps, presenting the full parameter covariance matrix in absolute units for any noise regime. With this, we make quantitative comparisons among the many various linear and full Stokes polarimeter designs, and in particular the less common designs that incorporate diattenuating detectors, highlighting the fact that the covariance matrices of optimized polarimeters take on a similar form in both IG and PP noise.

2. LINEAR STOKES POLARIMETERS

Linear Stokes polarimeters estimate only the first three parameters (s_0, s_1, s_2) of the full Stokes vector (s_0, s_1, s_2, s_3), i.e., those states corresponding to linear polarization. A division-of-time (DoT) linear Stokes polarimeter of this sort employs a single rotating polarizer [Fig. 1(a)], whereas a typical division-of-focal-plane polarimeter (DoFP) employs a tiled layout of micropolarizers placed on top of the detector array [Figs. 1(b)–1(e)] [5]. These two system layouts produce identical measurement matrices, and so we will not need to distinguish between the two in the following analysis. Rather, we will distinguish between the polarizer angles used to measure, starting with the most common choice of using the angles $\theta = 0°$, 45°, 90°, and 135° [i.e., Fig. 1(b)].

Using Mueller calculus, we can model the intensity I measured at the detector for any given input polarization state $\mathbf{s}$. For a polarizer oriented at one of the orientation angles 0°, 45°, 60°, 90°, 120°, or 135°, we find

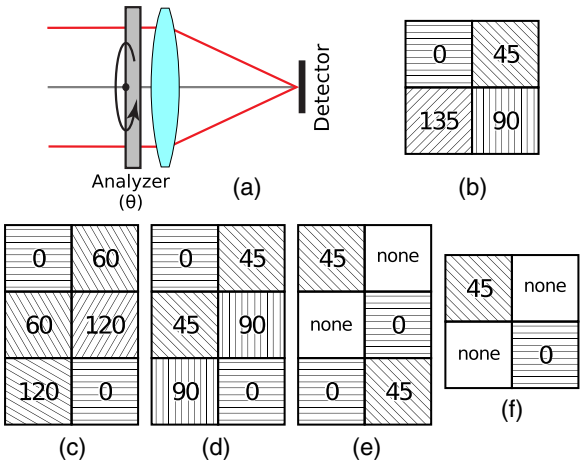

Fig. 1. Two methods for linear Stokes polarimetry: (a) rotating analyzer, and (b)–(f) tile of micropolarizer elements, arranged at orientations (b) 0-45-90-135, (c) 0-60-120, and (d) 0-45-90, and two methods mixing measurements with and without polarizer elements: (e) N-0-45, and (f) N-N-0-45.

$$
\begin{aligned}
I_0 &= \frac{\epsilon}{2}(s_0 + s_1) + n_0,\\
I_{45} &= \frac{\epsilon}{2}(s_0 + s_2) + n_{45},\\
I_{60} &= \frac{\epsilon}{2}\left(s_0 - \frac{1}{2}s_1 + \frac{\sqrt{3}}{2}s_2\right) + n_{60},\\
I_{90} &= \frac{\epsilon}{2}(s_0 - s_1) + n_{90},\\
I_{120} &= \frac{\epsilon}{2}\left(s_0 - \frac{1}{2}s_1 - \frac{\sqrt{3}}{2}s_2\right) + n_{120},\\
I_{135} &= \frac{\epsilon}{2}(s_0 - s_2) + n_{135},
\end{aligned}
\tag{1}
$$

where each measurement I_i is accompanied by a noise term n_i, and ϵ represents the polarimeter's detection efficiency. For an ideal lossless optical system, ϵ is equal to the detector quantum efficiency, whereas for a real system, it can be described as the "external quantum efficiency"—the ratio of detected photoelectrons per unit photon entering the optical system's entrance pupil.

Two of the configurations that we will consider later employ a measurement with the polarizer removed, in which case the model for the measured intensity is

$$I_{\text{none}} = s_0 + n_z.$$

In the analysis to follow, we will assume all of the noise terms to have zero mean, i.e., $\langle I_i\rangle = I_i$ and $\langle n_i\rangle = 0$. This causes no difficulties for Poisson-distributed noise, because our definition of the signal I and noise n results in the mean value of the Poisson-distributed variable to be incorporated into I, whereas n retains the zero-mean stochastic portion.

For photometric measurements, the most convenient unit with which to model Poisson noise contributions is light "intensity" such that s_0 represents the number of photons incident on the entrance pupil of the instrument during the measurement integration time. Poisson noise itself is parameterized by the photoelectron count rather than the photon count, with the proportionality between the two being the external quantum efficiency ϵ. Whereas the former (photon counts) is required to compare instruments with differing quantum efficiencies, the latter parameterizes the noise level. For IG noise, the measurement model can be more flexible because it is not signal dependent, allowing s_0 to take on arbitrary units, as long as the noise parameter shares the same choice of scaling.

A. 0-45-90-135 Configuration

In the case of the 0-45-90-135 configuration, we sample the input light at the four angles $\theta = 0°$, 45°, 90°, and 135°, which we can collect into matrix form as

$$
\underbrace{\begin{pmatrix} I_0\\ I_1\\ I_2\\ I_3\end{pmatrix}}_{\mathbf{I}} = \underbrace{\frac{\epsilon}{2}\begin{pmatrix} 1 & 1 & 0 & 0\\ 1 & 0 & 1 & 0\\ 1 & -1 & 0 & 0\\ 1 & 0 & -1 & 0\end{pmatrix}}_{\mathbf{W}} \underbrace{\begin{pmatrix} s_0\\ s_1\\ s_2\\ s_3\end{pmatrix}}_{\mathbf{s}} + \underbrace{\begin{pmatrix} n_0\\ n_1\\ n_2\\ n_3\end{pmatrix}}_{\mathbf{n}},
$$

or $\mathbf{I} = \mathbf{W}\mathbf{s} + \mathbf{n}$. Here, $\mathbf{W}$ is generally called the measurement matrix. By inspection, we can form estimators for the input Stokes vector elements as

$$
\begin{aligned}
\hat{s}_0 &= \frac{1}{2\epsilon}(I_0 + I_{45} + I_{90} + I_{135}),\\
\hat{s}_1 &= \frac{1}{\epsilon}(I_0 - I_{90}),\\
\hat{s}_2 &= \frac{1}{\epsilon}(I_{45} - I_{135}),
\end{aligned}
$$

which we can rewrite in matrix form as

$$
\underbrace{\begin{pmatrix} \hat{s}_0\\ \hat{s}_1\\ \hat{s}_2\\ \hat{s}_3\end{pmatrix}}_{\hat{\mathbf{s}}} = \underbrace{\frac{1}{2\epsilon}\begin{pmatrix} 1 & 1 & 1 & 1\\ 2 & 0 & -2 & 0\\ 0 & 2 & 0 & -2\\ 0 & 0 & 0 & 0\end{pmatrix}}_{\mathbf{A}} \underbrace{\begin{pmatrix} I_0\\ I_1\\ I_2\\ I_3\end{pmatrix}}_{\mathbf{I}}
\tag{2}
$$

or $\hat{\mathbf{s}} = \mathbf{A}\mathbf{I}$, where $\mathbf{A}$ is the analysis matrix—sometimes referred to as the synthesis matrix or the polarimetric data reduction matrix [6]. We use a hat (^) over any parameter that represents an estimate of a quantity. Thus $\hat{s}_i$ is a stochastic variable, as its value depends on the measurements, and therefore also on the noise, whereas s_i is deterministic (noise free).

Taking the expectation value of each estimator, we confirm that they provide unbiased estimates of the Stokes vectors, i.e., $\langle\hat{s}_i\rangle = s_i$. For the parameter measurement statistics, we next need to determine the variances, from which we can readily calculate the SNR values. Using the standard formula for variance, we can write, for each s_i,

$$\text{var}(s_i) = \langle\hat{s}_i^2\rangle - \langle s_i\rangle^2 = \langle\hat{s}_i^2\rangle - s_i^2. \tag{3}$$

We start with $\hat{s}_0$ and solve for the second moment, substituting in our definitions for the measurement terms I_i and the input (deterministic) Stokes vector elements s_i into the estimator:

$$\begin{aligned}\langle \hat{s}_0^2\rangle &= \left\langle \frac{1}{4\epsilon^2}(I_0+I_{45}+I_{90}+I_{135})^2 \right\rangle \\ &= \frac{1}{4\epsilon^2}\langle [2\epsilon s_0 + n_0 + n_{45} + n_{90} + n_{135}]^2\rangle \\ &= \frac{1}{4\epsilon^2}\langle 4\epsilon^2 s_0^2 + 4\epsilon s_0 n_0 + 4\epsilon s_0 n_{45} + 4\epsilon s_0 n_{90} + 4\epsilon s_0 n_{135} \\ &\quad + n_0^2 + n_{45}^2 + n_{90}^2 + n_{135}^2 + 2n_0 n_{45} + 2n_0 n_{90} \\ &\quad + 2n_0 n_{135} + 2n_{45} n_{90} + 2n_{45} n_{135} + 2n_{90} n_{135}\rangle \\ &= \frac{1}{4\epsilon^2}[4\epsilon^2 s_0^2 + \langle n_0^2\rangle + \langle n_{45}^2\rangle + \langle n_{90}^2\rangle + \langle n_{135}^2\rangle \\ &\quad + 2\langle n_0 n_{45}\rangle + 2\langle n_0 n_{90}\rangle + 2\langle n_0 n_{135}\rangle \\ &\quad + 2\langle n_{45} n_{90}\rangle + 2\langle n_{45} n_{135}\rangle + 2\langle n_{90} n_{135}\rangle]. \end{aligned} \tag{4}$$

We show this derivation in detail to make clear that at this point, we have made no assumptions on the statistical distribution of the noise, other than the fact that the noise samples have well-defined mean and variance. Correlated noise causes no difficulty up to this point, and any noise distributions (not just Poisson or Gaussian) with finite mean and variance values are valid within this analysis [7]. However, to simplify the analysis, we make our first substantial assumptions about the characteristics of the noise: (1) that the noise terms all share the same variance ($\langle n_i^2\rangle = \langle n_j^2\rangle \equiv \langle n^2\rangle$), and (2) that the noise terms are independent of one another ($\langle n_i n_j\rangle = \langle n_i\rangle\langle n_j\rangle$). This latter assumption in particular is useful, in that all mixed moments, due to the zero-mean property of the noise, become zero:

$$\langle \hat{s}_0^2\rangle = s_0^2 + \frac{1}{\epsilon^2}\langle n^2\rangle,$$

so that

$$\mathrm{var}(\hat{s}_0) = \frac{1}{\epsilon^2}v_\mathrm{d},$$

where we define $v_\mathrm{d} = \langle n^2\rangle$ as the variance of the measurement noise.

Performing a similar calculation for the second and third Stokes parameters, we obtain similar expressions:

$$\mathrm{var}(\hat{s}_1) = \frac{2}{\epsilon^2}v_\mathrm{d}, \qquad \mathrm{var}(\hat{s}_2) = \frac{2}{\epsilon^2}v_\mathrm{d}.$$

Likewise, calculating the covariances among the parameter estimates follows along a similar path:

$$\mathrm{cov}(\hat{s}_0,\hat{s}_1) = \langle(\hat{s}_0 - s_0)(\hat{s}_1 - s_1)\rangle = \langle \hat{s}_0\hat{s}_1\rangle - s_0 s_1.$$

So we proceed to calculate the joint moment

$$\begin{aligned}\langle \hat{s}_0\hat{s}_1\rangle &= \left\langle \frac{1}{2\epsilon}(I_0+I_{45}+I_{90}+I_{135})\cdot\frac{1}{\epsilon}(I_0+I_{90})\right\rangle \\ &= s_0 s_1 + \frac{1}{\epsilon^2}\langle n^2\rangle,\end{aligned}$$

where we have skipped the intermediate steps this time. From this we obtain the covariance:

$$\mathrm{cov}(\hat{s}_0,\hat{s}_1) = \frac{1}{\epsilon^2}v_\mathrm{d}.$$

By symmetry, we can also conclude that

$$\mathrm{cov}(\hat{s}_0,\hat{s}_2) = \frac{1}{\epsilon^2}v_\mathrm{d}.$$

The remaining covariance element cannot be obtained by symmetry arguments alone, but calculation gives $\langle \hat{s}_1,\hat{s}_2\rangle = 0$, so that we can form the full covariance matrix $\mathbf{K}$ of our estimators:

$$\begin{aligned}\mathbf{K}_\mathrm{IG} &= \begin{pmatrix} \mathrm{var}(\hat{s}_0) & \mathrm{cov}(\hat{s}_0,\hat{s}_1) & \mathrm{cov}(\hat{s}_0,\hat{s}_2) \\ \mathrm{cov}(\hat{s}_1,\hat{s}_0) & \mathrm{var}(\hat{s}_1) & \mathrm{cov}(\hat{s}_1,\hat{s}_2) \\ \mathrm{cov}(\hat{s}_2,\hat{s}_0) & \mathrm{cov}(\hat{s}_2,\hat{s}_1) & \mathrm{var}(\hat{s}_2)\end{pmatrix} \\ &= \frac{v_\mathrm{d}}{\epsilon^2}\begin{pmatrix}1&1&1\\1&2&0\\1&0&2\end{pmatrix}.\end{aligned}$$

The EWV performance metric is obtained as the trace of $\mathbf{K}$.

For measurements taken in the detector-limited noise regime, such as IG noise, this covariance matrix tells us everything we can know about the second-order statistics of our estimated parameters.

B. Mixed Gaussian–Poisson Noise

To expand the preceding analysis to a more general noise regime, we need to form a model for each of our noise terms. In the shot-noise-limited regime, each noise term will be signal dependent, such that the variance of a Poisson-distributed noise variable equals its mean value. For each of the intensities in the measurement model [Eq. (1)], we can thus write the noise variances as

$$\left.\begin{aligned}\mathrm{var}(n_0) &= \tfrac{\epsilon}{2}(s_0+s_1)+v_\mathrm{d}\\ \mathrm{var}(n_{45}) &= \tfrac{\epsilon}{2}(s_0+s_2)+v_\mathrm{d}\\ \mathrm{var}(n_{90}) &= \tfrac{\epsilon}{2}(s_0-s_1)+v_\mathrm{d}\\ \mathrm{var}(n_{135}) &= \tfrac{\epsilon}{2}(s_0-s_2)+v_\mathrm{d}\\ \mathrm{var}(n_{60}) &= \tfrac{\epsilon}{2}(s_0-\tfrac{1}{2}s_1+\tfrac{\sqrt{3}}{2}s_2)+v_\mathrm{d}\\ \mathrm{var}(n_{120}) &= \tfrac{\epsilon}{2}(s_0-\tfrac{1}{2}s_1-\tfrac{\sqrt{3}}{2}s_2)+v_\mathrm{d}\\ \mathrm{var}(n_\mathrm{none}) &= \epsilon s_0 + v_\mathrm{d}\end{aligned}\right\}. \tag{5}$$

Here, we maintain our definition of v_d as the Gaussian-distributed (signal-independent) noise from the detector. From this mixed PG noise model [8,9], we can take the shot-noise-limited regime (PP noise) by taking the limit $v_\mathrm{d}\to 0$, or the detector-noise-limited regime (IG) by taking $v_\mathrm{d} \gg$ (everything else).

Calculating the variances and covariances under the PG noise model involves returning to Eq. (4) and substituting the appropriate variances [Eq. (5)] for each $\langle n_i^2\rangle$. Note that under PG noise, each independent realization of the noise is independent, so that once again all of the cross terms cancel:

$$\begin{aligned}\mathrm{var}(\hat{s}_0) &= \frac{1}{4\epsilon^2}\Big[\langle n_0^2\rangle + \langle n_{45}^2\rangle + \langle n_{90}^2\rangle + \langle n_{135}^2\rangle \\ &\quad + 2\langle n_0 n_{45}\rangle + 2\langle n_0 n_{90}\rangle + 2\langle n_0 n_{135}\rangle \\ &\quad + 2\langle n_{45} n_{90}\rangle + 2\langle n_{45} n_{135}\rangle + 2\langle n_{90} n_{135}\rangle\Big] \\ &= \frac{1}{4\epsilon^2}\left(\left[\frac{\epsilon}{2}(s_0+s_1)+v_\mathrm{d}\right] + \left[\frac{\epsilon}{2}(s_0+s_2)+v_\mathrm{d}\right]\right. \\ &\quad \left. + \left[\frac{\epsilon}{2}(s_0-s_1)+v_\mathrm{d}\right] + \left[\frac{\epsilon}{2}(s_0-s_2)+v_\mathrm{d}\right]\right) \\ &= \frac{1}{2\epsilon}s_0 + \frac{1}{\epsilon^2}v_\mathrm{d}.\end{aligned}$$

Solving for the remaining terms, we obtain the covariance matrix under the PG noise:

$$\mathbf{K}_{\mathrm{PG}} = \frac{1}{\epsilon}\begin{pmatrix} \frac{1}{2}s_0 + \frac{1}{\epsilon}v_{\mathrm{d}} & \frac{1}{2}s_1 & \frac{1}{2}s_2 \\ \frac{1}{2}s_1 & s_0 + \frac{2}{\epsilon}v_{\mathrm{d}} & 0 \\ \frac{1}{2}s_2 & 0 & s_0 + \frac{2}{\epsilon}v_{\mathrm{d}} \end{pmatrix},$$

from which we can clearly see the dependence of the measurements on the input state of polarization (SOP).

We can also rewrite the form of the covariance matrix for the limit of PP noise, giving

$$\mathbf{K}_{\mathrm{PP}} = \frac{s_0}{2\epsilon}\begin{pmatrix} 1 & \tilde{s}_1 & \tilde{s}_2 \\ \tilde{s}_1 & 2 & 0 \\ \tilde{s}_2 & 0 & 2 \end{pmatrix},$$

where the tilde ($\tilde{}$) represents a normalized parameter: $\tilde{s}_i \equiv s_i/s_0$. The matrix diagonal, and thus the EWV, has exactly the same form here as it did for IG noise, with the only difference being the scale factor in front.

From the estimated variances, we can calculate the SNR of each of the Stokes parameters:

$$\mathrm{SNR}(\hat{s}_0) = \frac{s_0}{[\mathrm{var}(\hat{s}_0)]^{1/2}} = \frac{s_0}{\left(\frac{1}{2\epsilon}s_0 + \frac{1}{\epsilon^2}v_{\mathrm{d}}\right)^{1/2}},$$

which in the IG and PP noise regimes becomes

$$\mathrm{SNR}_{\mathrm{IG}}(\hat{s}_0) = \epsilon s_0/\sigma_{\mathrm{d}}, \quad \text{and} \quad \mathrm{SNR}_{\mathrm{PP}}(\hat{s}_0) = \sqrt{2\epsilon s_0},$$

where σ_{d} is the detector noise standard deviation, i.e., $\sigma_{\mathrm{d}} = \sqrt{v_{\mathrm{d}}}$. In accordance with what we expect, the SNR shows an increase with higher detection efficiency ϵ and with more light s_0.

Likewise, calculating the SNRs for $\hat{s}_1$ and $\hat{s}_2$ gives

$$\mathrm{SNR}_{\mathrm{IG}}(\hat{s}_1) = \epsilon s_1/\left(\sqrt{2}\sigma_{\mathrm{d}}\right), \quad \text{and} \quad \mathrm{SNR}_{\mathrm{PP}}(\hat{s}_1) = \tilde{s}_1\sqrt{\epsilon s_0}$$

and

$$\mathrm{SNR}_{\mathrm{IG}}(\hat{s}_2) = \epsilon s_2/\left(\sqrt{2}\sigma_{\mathrm{d}}\right), \quad \text{and} \quad \mathrm{SNR}_{\mathrm{PP}}(\hat{s}_2) = \tilde{s}_2\sqrt{\epsilon s_0}.$$

C. Matrix Approach for Calculating the Covariance Matrix

Although we have derived the variances and SNRs using the definition of the variance [Eq. (3)], we can calculate the covariance matrix directly from the measurement and analysis matrices. The covariance matrix $\mathbf{K}$ of Stokes vector elements can be written in terms of the analysis matrix $\mathbf{A}$ as

$$\mathbf{K} = \mathbf{A}\Gamma\mathbf{A}^{\mathrm{T}}, \tag{6}$$

where Γ is the covariance matrix of the raw detector measurements I_i. Under IG, PG, and PP noise, Γ is diagonal of the form

$$\Gamma = \begin{pmatrix} \mathrm{var}(n_0) & 0 & \dots & 0 \\ 0 & \mathrm{var}(n_1) & \dots & 0 \\ \vdots & \vdots & \ddots & \vdots \\ 0 & 0 & \dots & \mathrm{var}(n_M) \end{pmatrix},$$

or, under IG noise, simply

$$\Gamma_{\mathrm{IG}} = v_{\mathrm{d}}\mathbf{I},$$

for $M \times M$ identity matrix $\mathbf{I}$. In indicial form, Eq. (6) becomes [10]

$$K_{ij} = \left[\sum_{k=0}^{3} s_k \sum_{\ell=0}^{L-1} A_{i\ell}A_{j\ell}W_{\ell k}\right] + \left[v_{\mathrm{d}}\sum_{\ell=0}^{L-1} A_{i\ell}A_{j\ell}\right], \tag{7}$$

where L is the number of measurements (the number of rows in $\mathbf{W}$). An advantage of the indicial form is that we can write the result directly in terms of the measurement matrix $\mathbf{W}$ without having to first form Γ. The result, Eq. (7), differs from that of Goudail [10] by the addition of the Gaussian term $[v_{\mathrm{d}}\sum A_{i\ell}A_{j\ell}]$.

Something that must be kept in mind when working with the covariance matrices is that for singular $\mathbf{A}$, the covariance matrix is in general not singular. Rather, one will typically see that two of the parameters will be fully correlated with one another, with covariance elements equal in magnitude to the variances along the diagonal. Whereas the 2-norm condition number κ_2 of a singular matrix goes to infinity, giving a clear indication of a problem, this behavior in the covariance matrix is more subtle, requiring that one look carefully at the structure of the matrix to spot the singular structure. Thus, κ_2 is often a convenient supplement to covariance analysis.

D. 0-60-120 Configuration

Using the same methods, we can calculate the covariances for other polarimeter configurations. Bernard and Wehner, e.g., determined that the optimal set of three linear analyzer angles for estimating the linear Stokes vector is $\{0°, 60°, 120°\}$ [shown in Fig. 1(c)] [11,12]. For this "0-60-120" configuration, the three measurements take the form

$$I_0 = \frac{\epsilon}{2}(s_0 + s_1) + n_0,$$

$$I_{60} = \frac{\epsilon}{2}\left(s_0 - \frac{1}{2}s_1 + \frac{\sqrt{3}}{2}s_2\right) + n_{60}, \quad \text{and}$$

$$I_{120} = \frac{\epsilon}{2}\left(s_0 - \frac{1}{2}s_1 - \frac{\sqrt{3}}{2}s_2\right) + n_{120},$$

so that the measurement matrix $\mathbf{W}$, analysis matrix $\mathbf{A}$, and PG noise covariance matrix $\mathbf{K}$ are obtained as

$$\mathbf{W} = \frac{\epsilon}{2}\begin{pmatrix} 1 & 1 & 0 & 0 \\ 1 & -\frac{1}{2} & \frac{\sqrt{3}}{2} & 0 \\ 1 & -\frac{1}{2} & -\frac{\sqrt{3}}{2} & 0 \end{pmatrix}, \qquad \mathbf{A} = \frac{2}{\epsilon}\begin{pmatrix} \frac{1}{3} & \frac{1}{3} & \frac{1}{3} \\ \frac{2}{3} & -\frac{1}{3} & -\frac{1}{3} \\ 0 & \frac{1}{\sqrt{3}} & -\frac{1}{\sqrt{3}} \\ 0 & 0 & 0 \end{pmatrix},$$

and

$$\mathbf{K}_{\mathrm{PG}} = \frac{2}{3\epsilon}\begin{pmatrix} s_0 + \frac{2}{\epsilon}v_{\mathrm{d}} & s_1 & s_2 \\ s_1 & 2s_0 + s_1 + \frac{4}{\epsilon}v_{\mathrm{d}} & -s_2 \\ s_2 & -s_2 & 2s_0 - s_1 + \frac{4}{\epsilon}v_{\mathrm{d}} \end{pmatrix}.$$

Here, we see that whereas the variances of $\hat{s}_1$ and $\hat{s}_2$ in the 0-45-90-135 configuration are independent of the input SOP, the variances for the 0-60-120 setup have the curious property that they depend on the input state of s_1 but not of s_2. This is a feature of the 0-60-120 that we have also observed experimentally in our lab.

E. N-0-45 and N-N-0-45 Configurations

With a DoFP polarimeter in mind, Perkins and Gruev argued that an optimal four-measurement configuration can be achieved with one fully transmissive filter (i.e., no polarizer) plus just two polarizer angles of 0° and 45° [Fig. 1(e)] [13]. This setup can also be used to estimate the linear Stokes vector using only three measurements, and so we start with the three-measurement form and continue on to Perkins's suggested four-measurement system. For this "N-0-45" configuration [Fig. 1(e)], the three measurements take the form

$$I_{\mathrm{N}} = \epsilon s_0 + n_z,$$
$$I_0 = \frac{\epsilon}{2}(s_0 + s_1) + n_0, \quad \text{and}$$
$$I_{45} = \frac{\epsilon}{2}(s_0 + s_2) + n_{45},$$

so that the measurement, analysis, and covariance matrices are obtained as

$$\mathbf{W} = \varepsilon \begin{pmatrix} 1 & 0 & 0 & 0 \\ \frac{1}{2} & \frac{1}{2} & 0 & 0 \\ \frac{1}{2} & 0 & \frac{1}{2} & 0 \end{pmatrix}, \qquad \mathbf{A} = \frac{1}{\varepsilon} \begin{pmatrix} 1 & 0 & 0 \\ -1 & 2 & 0 \\ -1 & 0 & 2 \\ 0 & 0 & 0 \end{pmatrix},$$

and

$$\mathbf{K}_{\mathrm{PG}} = \frac{1}{\epsilon} \begin{pmatrix} s_0 + \frac{1}{\epsilon} v_{\mathrm{d}} & -s_0 - \frac{1}{\epsilon} v_{\mathrm{d}} & -s_0 - \frac{1}{\epsilon} v_{\mathrm{d}} \\ -s_0 - \frac{1}{\epsilon} v_{\mathrm{d}} & 3s_0 + 2s_1 + \frac{5}{\epsilon} v_{\mathrm{d}} & s_0 + \frac{1}{\epsilon} v_{\mathrm{d}} \\ -s_0 - \frac{1}{\epsilon} v_{\mathrm{d}} & s_0 + \frac{1}{\epsilon} v_{\mathrm{d}} & 3s_0 + 2s_2 + \frac{5}{\epsilon} v_{\mathrm{d}} \end{pmatrix}.$$

Perkins's original four-measurement system [Fig. 1(f)] uses two samples without a polarizer, producing the measurement equation and covariance matrix

$$\mathbf{K}_{\mathrm{PG}} = \frac{1}{2\epsilon} \begin{pmatrix} s_0 + \frac{1}{\epsilon} v_{\mathrm{d}} & -s_0 - \frac{1}{\epsilon} v_{\mathrm{d}} & -s_0 - \frac{1}{\epsilon} v_{\mathrm{d}} \\ -s_0 - \frac{1}{\epsilon} v_{\mathrm{d}} & 5s_0 + 2s_1 + \frac{9}{\epsilon} v_{\mathrm{d}} & s_0 + \frac{1}{\epsilon} v_{\mathrm{d}} \\ -s_0 - \frac{1}{\epsilon} v_{\mathrm{d}} & s_0 + \frac{1}{\epsilon} v_{\mathrm{d}} & 5s_0 + 2s_2 + \frac{9}{\epsilon} v_{\mathrm{d}} \end{pmatrix},$$

where we see that the variance of $\hat{s}_0$ and all of the off-diagonal terms have been halved, but the variances of $\hat{s}_1$ and $\hat{s}_2$ have been reduced by somewhat less than that.

Finally, it is interesting to see the consequences of getting by with only three of the original four polarizers in a conventional polarization camera, leaving only the 0°, 45°, and 90° polarizers [Fig. 1(d)]. The measurement, analysis, and covariance matrices are obtained as

$$\mathbf{W} = \frac{\epsilon}{2} \begin{pmatrix} 1 & 1 & 0 & 0 \\ 1 & 0 & 1 & 0 \\ 1 & -1 & 0 & 0 \end{pmatrix}, \qquad \mathbf{A} = \frac{1}{\epsilon} \begin{pmatrix} 1 & 0 & 1 \\ 1 & 0 & -1 \\ -1 & 2 & -1 \\ 0 & 0 & 0 \end{pmatrix},$$

and

$$\mathbf{K}_{\mathrm{PG}} = \frac{1}{\epsilon} \begin{pmatrix} s_0 + \frac{2}{\epsilon} v_{\mathrm{d}} & s_1 & -s_0 - \frac{2}{\epsilon} v_{\mathrm{d}} \\ s_1 & s_0 + \frac{2}{\epsilon} v_{\mathrm{d}} & -s_1 \\ -s_0 - \frac{2}{\epsilon} v_{\mathrm{d}} & -s_1 & 3s_0 + 2s_2 + \frac{6}{\epsilon} v_{\mathrm{d}} \end{pmatrix}.$$

3. COMPARISONS OF LINEAR STOKES POLARIMETERS

The Stokes parameter covariance matrix represents the complete statistical information we have about the parameter estimates up to second order, providing an ideal metric to evaluate and compare system performance. In particular, the advantages that the covariance matrix has over the widely used matrix condition number κ, or the EWV, are the following.

1. κ is invariant to detection efficiency ϵ, so that a comparison of systems having different efficiencies must incorporate an additional metric.
2. κ alone cannot be scaled to give the SNR of a polarimetric measurement.
3. κ does not provide information on the dependence of SNR on the input SOP.
4. Both κ and EWV combine all of the Stokes vector estimation characteristics into one metric, obscuring information on the differences in variance among the parameters as well as correlations between estimates.

Table 1. Compiled Variance Results for the Five Linear Stokes Polarimeter Configurations[a]

Configuration	var($\hat{s}_0$)	var($\hat{s}_1$)	var($\hat{s}_2$)	EWV	κ_1	κ_2	κ_∞	κ_{F}
IG Regime: □ $v_{\mathrm{d}}/\epsilon^2$								
0-45-90-135	1	2	2	5	3.00	1.41	2.00	3.16
0-60-120	4/3	8/3	8/3	20/3	3.73	1.41	3.15	3.16
0-45-90	2	2	6	10	4.50	2.41	4.00	3.87
N-0-45	1	5	5	11	6.00	3.19	3.00	4.69
N-N-0-45	1/2	9/2	9/2	19/2	6.00	3.61	3.00	5.34
PP Regime: □ s_0/ϵ								
0-45-90-135	$\frac{1}{2}$	1	1	$\frac{5}{2}$				
0-60-120[b]	$\frac{2}{3}$	$\frac{4}{3}+\frac{2}{3}\tilde{s}_1$	$\frac{4}{3}+\frac{2}{3}\tilde{s}_1$	$\frac{10}{3}+\frac{4}{3}\tilde{s}_1$				
0-45-90	1	1	$3+2\tilde{s}_2$	$5+2\tilde{s}_2$				
N-0-45	1	$\frac{3}{2}+\tilde{s}_1$	$\frac{3}{2}+\tilde{s}_2$	$4+\tilde{s}_1+\tilde{s}_2$				
N-N-0-45	$\frac{1}{4}$	$\frac{5}{4}+\tilde{s}_1$	$\frac{5}{4}+\frac{1}{2}\tilde{s}_2$	$\frac{11}{4}+\tilde{s}_1+\frac{1}{2}\tilde{s}_2$				

[a]Each of the IG regime entries (□) share a $v_{\mathrm{d}}/\epsilon^2$ factor, whereas each of the PP regime entries (□) share a s_0/ϵ factor.
[b]The dependence on $\tilde{s}_1$ in the var($\hat{s}_2$) column is not a typo.

The variances for the linear Stokes polarimeter configurations are listed in Table 1 for easy comparison. From the table, we see that the smallest variances are achieved for the conventional 0-45-90-135 configuration and for the N-N-0-45 system. However, because these two use four measurements to the other systems' three, they can be considered as unfairly rewarded and so should be scaled by a factor of 4/3 to apply to working with the same number of photons. Applying this scale factor, we find that all of the variances of the 0-45-90-135 and the 0-60-120 configurations are identical under IG noise. They do not, however, have the same covariances (the off-diagonal elements).

Farther down in Table 1, we see differences among the configurations showing up in the PP regime. Thus, in PP noise, whereas the 0-45-90-135 and 0-60-120 configurations perform equivalently when $\tilde{s}_1 = 0$ (when scaled to compensate for the differences in the number of measurements), the 0-60-120 system's performance worsens as $\tilde{s}_1$ increases from zero toward 1 and improves as $\tilde{s}_1$ decreases from zero toward −1. Note that the dependence on $\tilde{s}_1$ in the var($\hat{s}_2$) is not a typo. Whereas the performances of the two systems remain the same on average, they are not the same for any specific measurement except when $\tilde{s}_1 = 0$.

For the other polarimeter configurations shown in Table 1, we see that the N-0-45 and N-N-0-45 configurations have good performance for estimating s_0, which should be no surprise, but that they make a heavy sacrifice in performance for estimating s_1 and s_2, producing variances that are more than twice as high. In addition, we see that the 0-45-90 configuration, by dropping the fourth measurement, has doubled the variance in $\hat{s}_0$ and tripled it in $\hat{s}_2$. More complex relationships develop under PP noise, but the basic trend remains.

Whereas the polarimeters considered here use single-channel polarization detection, so that half of the input light is lost, DoT (but not DoFP) implementations can improve the efficiency by a factor of 2 by using a polarization beam splitter and two detection channels. This can be used to either double the amount of light collected, effectively removing the factor of 1/2 at the front of each measurement matrix, or halving the number of measurements required. Doubling the number of measurements also causes a doubling of the detector noise v_d.

The equivalent performance of the 0-60-120 and 0-45-90-135 configurations supports the following conclusion reached by several researchers: if the configuration is optimal, there is no noise benefit to spreading the measurements to sample the measurement space more evenly [1,3,14]. This property is confirmed by the covariance matrices in Table 1, where we also see that the equivalence holds true in general for IG noise, but it holds in PP noise only when averaging the performance across all polarization states. Running a simulation over all configurations that sample the half-circle evenly at up to 360 angles, we confirmed that the equivalence holds for all such configurations, once normalized by the number of measurements taken.

Whereas Tyo concurred with this result [3], he also pointed out that instrument robustness to calibration error and perturbation improves with use of more sampling angles, so that there is some trade-off between noise performance and robustness.

The SNR values corresponding to the parameter variances are listed in Table 2.

Table 2. Compiled SNR Results for the Five Linear Stokes Polarimeter Configurations[a]

Configuration	SNR($\hat{s}_0$)	SNR($\hat{s}_1$)	SNR($\hat{s}_2$)
	IG Regime: □ $\epsilon s_0/\sigma_d$		
0-45-90-135	1	$0.707\tilde{s}_1$	$0.707\tilde{s}_2$
0-60-120	0.866	$0.612\tilde{s}_1$	$0.612\tilde{s}_2$
0-45-90	0.707	$0.707\tilde{s}_1$	$0.408\tilde{s}_2$
N-0-45	1	$0.447\tilde{s}_1$	$0.447\tilde{s}_2$
N-N-0-45	1.414	$0.471\tilde{s}_1$	$0.471\tilde{s}_2$
	PP Regime: □ $\sqrt{\epsilon/s_0}$		
0-45-90-135	1.414	s_1	s_2
0-60-120	0.866	$\frac{1.732}{\sqrt{2+\tilde{s}_1}}s_1$	$\frac{1.732}{\sqrt{2+\tilde{s}_1}}s_2$
0-45-90	1	s_1	$\frac{1}{\sqrt{3+2\tilde{s}_2}}s_2$
N-0-45	1	$\frac{1.414}{\sqrt{3+2\tilde{s}_1}}s_1$	$\frac{1.414}{\sqrt{3+2\tilde{s}_2}}s_2$
N-N-0-45	2	$\frac{2}{\sqrt{5+4\tilde{s}_1}}s_1$	$\frac{2}{\sqrt{5+2\tilde{s}_2}}s_2$

[a]Each of the IG regime entries (□) share a $\epsilon s_0/\sigma_d$ factor, whereas each of the PP regime entries (□) share a $\sqrt{\epsilon/s_0}$ factor.

4. ROTATING-RETARDER FULL STOKES POLARIMETERS

Whereas the discussion up to this point has focused on linear Stokes polarimetry, full Stokes polarimeters, estimating all four of the Stokes vector elements, occupy perhaps an even more important place in research work. The most widely used implementation for this is probably the rotating-retarder fixed-polarizer (RRFP) configuration, as shown in Fig. 2(a).

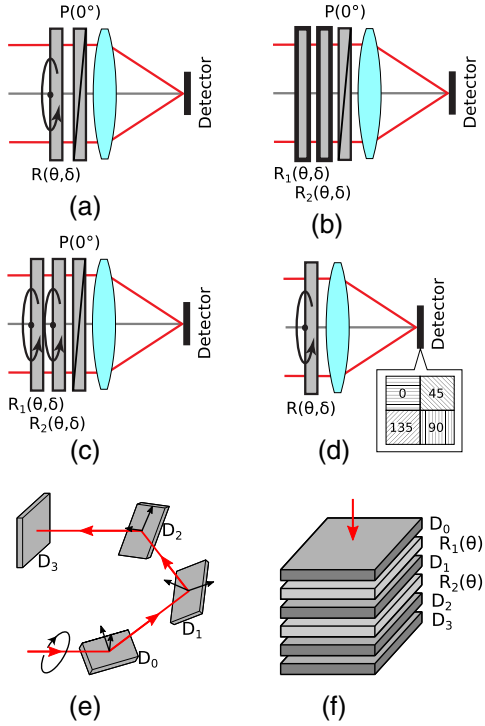

Fig. 2. Instrument layouts for (a) RRFP [15], (b) DVRFP [2], (c) DRRFP [16], (d) RRPC, (e) Azzam's four-detector polarimeter [17], and (f) diattenuator photovoltaic detector stack [18]. In each subfigure, R_i is the ith retarder, D_j the jth detector, and P the polarizer element.

Table 3. Instrument Configurations for Three RP Polarimeters, Where θ Indicates the Retarder Angle and ϕ the Polarizer Angle

Configuration	Measurement #	δ	θ	ϕ
Ambirajan	1	90°	−45°	0°
	2	90°	0°	0°
	3	90°	30°	0°
	4	90°	60°	0°
Sabatke	1	131.8°	−51.69°	0°
	2	131.8°	−15.12°	0°
	3	131.8°	15.12°	0°
	4	131.8°	51.69°	0°
Shibata	1	90°	22.5°	0°
	2	90°	22.5°	45°
	3	90°	22.5°	90°
	4	90°	22.5°	135°
	5	90°	67.5°	0°
	6	90°	67.5°	45°
	7	90°	67.5°	90°
	8	90°	67.5°	135°

Ambirajan and Look analyzed the best choice of azimuth angles for use with the RRFP system employing a quarter-wave retarder and found that the set of four angles −90°, −45°, 30°, and 60° are a good choice for minimizing the measurement matrix condition number [15]. Sabatke *et al.* considered simultaneously optimizing over angles and wave plate retardance δ, finding that the widely used choice of $\delta = 90°$ is in fact not optimal and that by choosing $\delta = 132°$, one can improve performance by about 50% [1].

A related configuration employs a rotating retarder in front of a 0-45-90-135 DoFP polarization camera. This system takes advantage of the four polarization angles simultaneously sampled at the detector array to collect the full Stokes vector image from only two retarder angles [19]. To our knowledge, the performance of this system has not yet been analyzed, despite its simplicity.

The configurations for the three RR polarimeters are tabulated in Table 3.

A. Ambirajan's RRFP

Applying Mueller calculus to Ambirajan's suggested instrument setup [15], we obtain the measured intensities as

$$I_0 = \frac{\epsilon}{2}(s_0 + s_1) + n_0,$$

$$I_1 = \frac{\epsilon}{2}(s_0 + s_3) + n_1,$$

$$I_2 = \frac{\epsilon}{2}\left(s_0 + \frac{1}{4}s_1 + \frac{\sqrt{3}}{4}s_2 - \frac{\sqrt{3}}{2}s_3\right) + n_2, \quad \text{and}$$

$$I_3 = \frac{\epsilon}{2}\left(s_0 + \frac{1}{4}s_1 - \frac{\sqrt{3}}{4}s_2 - \frac{\sqrt{3}}{2}s_3\right) + n_3$$

giving

$$\mathbf{W} = \epsilon \begin{pmatrix} \frac{1}{2} & \frac{1}{2} & 0 & 0 \\ \frac{1}{2} & 0 & 0 & \frac{1}{2} \\ \frac{1}{2} & \frac{1}{8} & \frac{\sqrt{3}}{8} & -\frac{\sqrt{3}}{4} \\ \frac{1}{2} & \frac{1}{8} & -\frac{\sqrt{3}}{8} & -\frac{\sqrt{3}}{4} \end{pmatrix}.$$

The full covariance matrix under PG noise is given in Table 7, which in the limit of IG noise becomes

$$\mathbf{K}_{\mathrm{IG}} = \frac{v_{\mathrm{d}}}{\epsilon^2} \begin{pmatrix} 2.01 & -2.63 & 0 & 0.13 \\ -2.63 & 7.25 & 0 & 0.49 \\ 0 & 0 & 10.67 & 0 \\ 0.13 & 0.49 & 0 & 1.72 \end{pmatrix}.$$

B. Sabatke's RRFP

The RRFP configuration optimized by Sabatke *et al.* [1], employing a $\delta = 132°$ wave plate at four azimuth angles, gives a measurement matrix of

$$\mathbf{W} = \epsilon \begin{pmatrix} 0.5 & 0.2888 & 0.3628 & -0.1869 \\ 0.5 & 0.2888 & -0.3628 & 0.1869 \\ 0.5 & -0.2897 & -0.1881 & -0.3615 \\ 0.5 & -0.2897 & 0.1881 & 0.3615 \end{pmatrix}.$$

The full covariance matrix under PG noise is given in Table 8, which in the limit of IG noise becomes

$$\mathbf{K}_{\mathrm{IG}} = \frac{v_{\mathrm{d}}}{\epsilon^2} \begin{pmatrix} 1 & 0 & 0 & 0 \\ 0 & 3 & 0 & 0 \\ 0 & 0 & 3 & 0 \\ 0 & 0 & 0 & 3 \end{pmatrix}.$$

We see that the covariances disappear under IG noise, and the s_1–s_3 parameter variances become uniform. In the limit of PP noise, the covariance matrix Table 8 becomes

$$\mathbf{K}_{\mathrm{PP}} = \frac{s_0}{2\epsilon} \begin{pmatrix} 1 & \tilde{s}_1 & \tilde{s}_2 & \tilde{s}_3 \\ \tilde{s}_1 & 3 & \tilde{s}_2 - \sqrt{2}\tilde{s}_3 & -\sqrt{2}\tilde{s}_2 - \tilde{s}_3 \\ \tilde{s}_2 & \tilde{s}_2 - \sqrt{2}\tilde{s}_3 & 3 & -\sqrt{2}\tilde{s}_1 \\ \tilde{s}_3 & -\sqrt{2}\tilde{s}_2 & -\sqrt{2}\tilde{s}_1 & 3 \end{pmatrix},$$

from which we see that the covariance matrix is no longer diagonal but that the matrix trace is identical to that of the IG case, up to a scalar factor. In fact, this pattern of 1:3:3:3 ratios of variances along the diagonal is retained in the full PG matrix, a feature shared by all of the optimized polarimeter designs, as we will see in the following.

C. Shibata's Rotating-Retarder Polarization Camera

Shibata *et al.* adapted a standard 0-45-90-135 configuration DoFP linear Stokes polarimeter to full Stokes polarimetry by inserting a rotating quarter-wave plate in front and rotating to two azimuth angle (θ) positions [19]. It is useful to look into the performance of this system in comparison to others due to its simplicity and to the increasing availability of these DoFP cameras. Unfortunately, the polarization camera cannot be converted into a snapshot full Stokes polarimeter with the addition of a fixed retarder in front, because this configuration can only generate a 2D subset of states on the Poincaré sphere, so that s_1 and s_2 cannot be separated from one another. Using a pair of retarder azimuth angles generates a set of eight measurements, which for $\theta = 22.5°$ and $67.5°$ gives the measurement matrix

$$\mathbf{W} = \frac{1}{4}\begin{pmatrix} 1 & \frac{1}{\sqrt{2}} & 0 & -\frac{1}{\sqrt{2}} \\ 1 & 0 & 1 & 0 \\ 1 & -\frac{1}{\sqrt{2}} & 0 & \frac{1}{\sqrt{2}} \\ 1 & 0 & -1 & 0 \\ 1 & 1 & 0 & 0 \\ 1 & 0 & 1 & 0 \\ 1 & -1 & 0 & 0 \\ 1 & 0 & -1 & 0 \end{pmatrix},$$

where we have normalized the matrix such that the first column of the matrix sums to 2, to agree with the overall light level implicit in the previous full Stokes polarimeters. The full PG-noise covariance matrix, which is simple enough to present here in its entirety, is

$$\mathbf{K}_{\mathrm{PG}} = \frac{1}{2\epsilon}\begin{pmatrix} s_0 + \frac{2}{\epsilon}v_d & s_1 & s_2 & s_3 \\ s_1 & 4s_0 + \frac{16}{\epsilon}v_d & 0 & 0 \\ s_2 & 0 & 4s_0 + \frac{16}{\epsilon}v_d & 0 \\ s_3 & 0 & 0 & 2s_0 + \frac{8}{\epsilon}v_d \end{pmatrix},$$

and which in IG noise takes on the particularly simple form

$$\mathbf{K}_{\mathrm{IG}} = \frac{v_{\mathrm{d}}}{\epsilon^2}\begin{pmatrix} 2 & 0 & 0 & 0 \\ 0 & 8 & 0 & 0 \\ 0 & 0 & 8 & 0 \\ 0 & 0 & 0 & 4 \end{pmatrix}.$$

From the covariance matrix, we can see that the normalization of the measurement matrix—multiplying $\mathbf{W}$ by 1/2 to set the overall amount of light sampled at $4s_0$—indicates that this system is less efficient with measuring the input light than the RRFP instruments are. However, one of the benefits of Shibata's approach is that it uses only two retarder positions to measure, which one can argue boosts its ability to collect light by a factor of 2, so that the parameter variances are reduced by a factor of 2 in IG noise, $\sqrt{2}$ in PP noise. With this scaling, the polarization camera-based system's performance is comparable to that of the RRFP instruments.

5. DUAL-RETARDER FULL STOKES POLARIMETERS

Whereas the previous systems used single-retarder elements with fixed retardance δ but variable orientation θ, another common setup for polarimetry is to use variable retarders, such as tunable liquid crystal retarders and acousto-optic modulators, which typically have fixed orientation. Because fast modulators, such as electro-, magneto-, and acousto-optic elements, typically use a more involved estimation procedure than the slower liquid crystal elements do, we will focus on the latter here.

Whereas single-variable-retarder elements have a limited ability to sample polarization space, dual-variable-retarder fixed-polarizer (DVRFP) systems can access a larger range of polarization states than the RRFP or rotating-retarder polarization-camera (RRPC) systems do [20]. Thus, they have a wider range of configurations capable of reaching optimal performance. An example given by Tyo [3] is analyzed in the next section, though many other optimized configurations are possible [21]. In a similar fashion, Zallat *et al.* demonstrate that using two dual-rotating-retarder fixed polarizers (DRRFPs) increases the flexibility of an RRFP polarimeter, and this system is analyzed in the following section [16].

Table 4. Instrument Configurations for the Variable Retarder Systems

Configuration	Measurement #	θ_1	δ_1	θ_2	δ_2
Tyo	1	22.5°	158°	45°	50.6°
	2	22.5°	127°	45°	−178°
	3	22.5°	47°	45°	−16.9°
	4	22.5°	0.66°	45°	126°
Zallat	1	−41.4°	90°	−20.3°	90°
	2	41.4°	90°	−20.3°	90°
	3	−41.4°	90°	20.3°	90°
	4	41.4°	90°	20.3°	90°

A. Tyo's DVRFP

Tyo's DVRFP configuration [2] is listed in Table 4 and gives a measurement matrix

$$\mathbf{W} = \epsilon\begin{pmatrix} 0.5 & -0.090789 & 0.408154 & 0.274167 \\ 0.5 & -0.089631 & -0.410064 & 0.271687 \\ 0.5 & 0.477507 & 0.000899 & -0.148277 \\ 0.5 & -0.297178 & 0.003285 & -0.402088 \end{pmatrix}.$$

This produces the full PG covariance matrix given in Table 9, converging to the following in the limit of IG noise:

$$\mathbf{K}_{\mathrm{IG}} = \frac{v_{\mathrm{d}}}{\epsilon^2}\begin{pmatrix} 1.00 & 0 & 0 & 0 \\ 0 & 3.01 & 0 & 0 \\ 0 & 0 & 2.99 & 0 \\ 0 & 0 & 0 & 3.01 \end{pmatrix}.$$

B. Zallat's DRRFP

Zallat *et al.* proposed a setup with a pair of rotating quarter-wave plates followed by a fixed polarizer (DRRFP) [16]. The configuration details are listed in Table 4, and the setup produces a measurement matrix

$$\mathbf{W} = \epsilon\begin{pmatrix} 0.5 & -0.287573 & -0.3198 & 0.255009 \\ 0.5 & 0.296629 & -0.248116 & -0.316938 \\ 0.5 & 0.296629 & 0.248116 & 0.316938 \\ 0.5 & -0.287573 & 0.319800 & -0.255009 \end{pmatrix}.$$

The full PG covariance matrix for this is given in Table 10, converging to the following in the limit of IG noise:

$$\mathbf{K}_{\mathrm{IG}} = \frac{v_{\mathrm{d}}}{\epsilon^2}\begin{pmatrix} 1.00 & 0 & 0 & 0 \\ 0 & 2.93 & 0 & 0 \\ 0 & 0 & 3.05 & 0 \\ 0 & 0 & 0 & 3.02 \end{pmatrix}.$$

6. IDEALIZED FULL STOKES POLARIMETERS

Iniesta and Collados introduced an alternative metric for evaluating polarimeter performance that they call the polarimetric

efficiency, from which they derive two idealized measurement matrices for maximizing their efficiency metric [22]. The first ideal matrix is a four-measurement scheme that was later presented by Goudail in the context of a ideal measurement in the presence of Poisson noise, apparently derived independently of Iniesta's work [10]. This is the first ideal system presented in the next section. Because Iniesta and Goudail both refer to the measurement matrix alone without discussing an instrument configuration capable of achieving it, we refer to this as an "idealized" polarimeter, though Mu *et al.* later demonstrated that this measurement can be achieved using a polarimeter with a fixed polarizer and a pair of rotating quarter-wave plates [23].

In addition to the first system, Iniesta and Collados also presented an idealized six-measurement system in which each of the Stokes s_1 through s_3 parameters is analyzed individually by a pair of measurements. This, they show, achieves the same polarimetric efficiency as the four-measurement ideal system, albeit at the cost of requiring an added two measurements.

Analyzing the performance of these two idealized systems provides an interesting view into the polarimetric design space.

A. Iniesta's Four-Measurement System

The first of Iniesta's idealized systems was identified by Goudail as having the special characteristic that its performance is independent of the input SOP. The system measurement matrix is

$$\mathbf{W} = \frac{\epsilon}{2\sqrt{3}} \begin{pmatrix} \sqrt{3} & 1 & -1 & -1 \\ \sqrt{3} & 1 & 1 & 1 \\ \sqrt{3} & -1 & 1 & -1 \\ \sqrt{3} & -1 & -1 & 1 \end{pmatrix},$$

for which the full PG covariance matrix $\mathbf{K}_{\mathrm{PG}}$ is shown in Table 11. In the limit of IG and PP noise regimes, $\mathbf{K}_{\mathrm{PG}}$ becomes

$$\mathbf{K}_{\mathrm{IG}} = \frac{v_{\mathrm{d}}}{\epsilon^2} \begin{pmatrix} 1 & 0 & 0 & 0 \\ 0 & 3 & 0 & 0 \\ 0 & 0 & 3 & 0 \\ 0 & 0 & 0 & 3 \end{pmatrix}$$

and

$$\mathbf{K}_{\mathrm{PP}} = \frac{s_0}{2\epsilon} \begin{pmatrix} 1 & \tilde{s}_1 & \tilde{s}_2 & \tilde{s}_3 \\ \tilde{s}_1 & 3 & \sqrt{3}\tilde{s}_3 & \sqrt{3}\tilde{s}_2 \\ \tilde{s}_2 & \sqrt{3}\tilde{s}_3 & 3 & \sqrt{3}\tilde{s}_1 \\ \tilde{s}_3 & \sqrt{3}\tilde{s}_2 & \sqrt{3}\tilde{s}_1 & 3 \end{pmatrix}.$$

Here we can see that this system achieves Goudail's aim of performance that is independent of the input SOP, but we do find that the off-diagonal covariances retain some SOP dependence.

B. Iniesta's Six-Measurement System

Although it was not identified as such by its authors, the second of Iniesta's systems also achieves the characteristic that its performance is independent of the input SOP. Though Iniesta and Collados did not identify instrumentation capable of achieving this measurement matrix, it is straightforward to see that a system such as that of Ref. [24] has an equivalent measurement matrix. This system employs a six-cell filter wheel in which pairs of cells contain vertical/horizontal polarizers, 45°/−45° polarizer, and right-circular/left-circular polarizers. To standardize the measurement to operate on a light input of $4s_0$, the first column of the measurement matrix is scaled to give a sum of 2 (reduced from 4 due to the polarizer rejecting half of the light).

For this system, the measurement matrix is

$$\mathbf{W} = \frac{\epsilon}{3} \begin{pmatrix} 1 & 1 & 0 & 0 \\ 1 & -1 & 0 & 0 \\ 1 & 0 & 1 & 0 \\ 1 & 0 & -1 & 0 \\ 1 & 0 & 0 & 1 \\ 1 & 0 & 0 & -1 \end{pmatrix},$$

giving a covariance matrix

$$\mathbf{K}_{\mathrm{PG}} = \frac{1}{2\epsilon} \begin{pmatrix} s_0 + \frac{3}{\epsilon} v_{\mathrm{d}} & s_1 & s_2 & s_3 \\ s_1 & 3s_0 + \frac{9}{\epsilon} v_{\mathrm{d}} & 0 & 0 \\ s_2 & 0 & 3s_0 + \frac{9}{\epsilon} v_{\mathrm{d}} & 0 \\ s_3 & 0 & 0 & 3s_0 + \frac{9}{\epsilon} v_{\mathrm{d}} \end{pmatrix},$$

which in the IG limit becomes

$$\mathbf{K}_{\mathrm{IG}} = \frac{v_{\mathrm{d}}}{\epsilon^2} \begin{pmatrix} \frac{3}{2} & 0 & 0 & 0 \\ 0 & \frac{9}{2} & 0 & 0 \\ 0 & 0 & \frac{9}{2} & 0 \\ 0 & 0 & 0 & \frac{9}{2} \end{pmatrix}.$$

7. DIATTENUATING FULL STOKES POLARIMETERS

Developing a photometric model for polarimetric measurement allows us to characterize the statistical behavior of systems having different detection efficiencies and, in particular, systems that incorporate diattenuating elements instead of ideal (or near-ideal) polarizer elements. The first system is Azzam's four-detector polarimeter [Fig. 2(e)], in which the incoming light is reflected off three detector elements oriented at specific orientation angles for each to act as diattenuators and partial detectors [17]. The light remaining after the third detector is absorbed at the fourth, placed at normal incidence to the beam. The following calculations are apparently the first to compare the performance of Azzam's system to other polarimetric techniques.

The second instrument we analyze is the stacked photovoltaic polarimeter developed by Kudenov *et al.* [Fig. 2(f)] [18,25]. This instrument consists of a stack of partially detecting organic photovoltaic elements sandwiched with wave plates. Here too we encounter an instrument employing diattenuator elements, so that quantitative comparison with other techniques requires use of a photometric model.

In both cases, researchers provide experimentally obtained measurement matrices rather than theoretical models, so that the detection efficiency ϵ is already incorporated into $\mathbf{W}$. We can also note that whereas most of the other polarimeter types scan in time to collect the four measurements needed to reconstruct the Stokes vector, Azzam's and Kudenov's instruments

split the input light among their four detectors. Thus, the diattenuating systems' measurement model naturally assumes the amount of light available for measurement is s_0 rather than $4s_0$. This artificially penalizes the noise in the reconstructed Stokes parameters. Thus, to compare performance under similar measurement assumptions, we augment the measurement matrices to assume $4s_0$ as input. This produces entries that are greater than 1 in the first column, which appears unphysical unless we keep in mind this scaling by a factor of 4.

A. Azzam's Four-Detector Polarimeter

The measurement matrix for the four-detector polarimeter is provided by Azzam in Ref. [26] as

$$\mathbf{W} = \begin{pmatrix} 0.746 & 0.157 & -0.071 & -0.001 \\ 2.433 & -1.180 & 0.516 & 0.447 \\ 0.694 & -0.244 & 0.137 & -0.405 \\ 2.597 & -1.934 & -0.296 & -0.429 \end{pmatrix}.$$

However, we can see that this matrix is not provided in photometric form—the sum of the entries in the first column is 6.47, which is unphysical for a photometric model. If we assume that the overall detection efficiency of this system approaches 1, and that the input light level is $4s_0$, then we can normalize the matrix to

$$\mathbf{W}^* = \begin{pmatrix} 0.461 & 0.097 & -0.044 & -0.001 \\ 1.504 & -0.730 & 0.319 & 0.276 \\ 0.429 & -0.151 & 0.085 & -0.250 \\ 1.606 & -1.196 & -0.183 & -0.265 \end{pmatrix}.$$

The full PG covariance matrix for $\mathbf{W}^*$ is shown in Table 12. In the limit of IG noise, the covariance matrix becomes

$$\mathbf{K}^*_{\mathrm{IG}} = v_{\mathrm{d}} \begin{pmatrix} 2.26 & 3.37 & -2.64 & 0.26 \\ 3.37 & 5.63 & -3.12 & -0.50 \\ -2.64 & -3.12 & 16.69 & -8.41 \\ 0.26 & -0.50 & -8.41 & 9.93 \end{pmatrix}.$$

Whereas the normalization of the measurement matrix has no effect on the condition numbers, it increases the PP-regime variances by 1.6 and the IG-regime variances by 2.6.

B. Kudenov's Stacked Photovoltaic Polarimeter

The measurement matrix for this system is provided by Yang *et al.* in Ref. [18] as

$$\mathbf{W} = \begin{pmatrix} 0.0753 & -0.0331 & 0 & 0 \\ 0.0280 & 0.0057 & -0.0046 & 0.0038 \\ 0.0105 & 0.0043 & 0.0042 & 0.0008 \\ 0.0045 & 0.0030 & -0.0001 & -0.0012 \end{pmatrix}.$$

However, as with Azzam's four-detector polarimeter, the reported matrix is also not given in photometric form, as its elements are given in units of amperes. If we normalize the matrix so that the first column sums to 4, we obtain

$$\mathbf{W}^* = \begin{pmatrix} 2.546 & -1.119 & 0.000 & 0.000 \\ 0.947 & 0.193 & -0.156 & 0.128 \\ 0.355 & 0.145 & 0.142 & 0.027 \\ 0.152 & 0.101 & -0.003 & -0.041 \end{pmatrix}.$$

This gives the covariance matrix shown in Table 13. In the limit of IG noise, the covariance matrix becomes

$$\mathbf{K}^*_{\mathrm{IG}} = v_{\mathrm{d}} \begin{pmatrix} 1.34 & 2.89 & -1.42 & -13.87 \\ 2.89 & 7.00 & -3.35 & -31.10 \\ -1.42 & -3.35 & 34.07 & 42.67 \\ -13.87 & -31.10 & 42.67 & 221.41 \end{pmatrix}.$$

Yang *et al.* are aware of the low performance that this system delivers, and they show that optimizing the photovoltaic element characteristics should provide a substantial improvement. They model an optimized measurement matrix as

$$\mathbf{W}^*_{\mathrm{II}} = \begin{pmatrix} 1.187 & -0.770 & -1.636 & 0.000 \\ 1.043 & 0.314 & -0.254 & -0.672 \\ 0.923 & 0.111 & 0.785 & 0.067 \\ 0.847 & 0.346 & -0.367 & 0.604 \end{pmatrix},$$

where we have normalized the matrix given in Ref. [18] into idealized photometric form. The corresponding covariance matrix is given in Table 14, which in the limit of IG noise becomes

$$[\mathbf{K}^*_{\mathrm{II}}]_{\mathrm{IG}} = v_{\mathrm{d}} \begin{pmatrix} 0.36 & -0.31 & 0.29 & 0.06 \\ -0.31 & 2.49 & -0.98 & -0.06 \\ 0.29 & -0.98 & 0.75 & 0.05 \\ 0.06 & -0.06 & 0.05 & 1.22 \end{pmatrix}.$$

In contrast to the Azzam instrument, the photometric normalization of the measurement matrix here has improved the results significantly. Without knowing the measurement model for this system in more detail, however, we cannot determine the correct scaling factor to use here. The low quantum efficiency and significant reflectivity of the photovoltaic detectors themselves means that, unlike the Azzam four-detector system, an assumption of ideal external quantum efficiency seems unrealistic [27].

8. COMPARISONS OF FULL STOKES POLARIMETERS

Table 5 shows the variances for all eight of the full Stokes polarimeter configurations, assuming that the total amount of light available for measurement is $4s_0$. To compensate for the fact that the Azzam and Kudenov system variances are for actual measurement matrices rather than for ideal measurement matrices, we used the efficiency-normalized (starred) versions of the measurement model here.

From the results shown in Table 5, we can clearly see the improvement of Sabatke's RRFP with $\delta = 132°$ in place of Ambirajan's use of the much more common quarter-wave plate ($\delta = 90°$). Ambirajan's setup appears to be particularly good at measuring circular states (s_3), at which it surpasses all of the optimized systems.

The results also show that all of the instruments in the middle of the table—Sabatke's RRFP, Tyo's DVRFP, Zallat's DRRFP, and Iniesta's two idealized systems—enjoy optimal performance, in which the parameter variances give a 1:3:3:3 ratio, not only just in IG noise but across all noise regimes (PG regime). Goudail proposed the system labeled here as "Iniesta-4" as having the unique properties of having homogeneous noise properties independent of the input SOP, but we can see that this is in fact a property shared by all of the optimized designs [10]. Thus, due to the generality of the derivation, it appears that any polarimeter optimized under IG noise is simultaneously optimized in any noise regime that

Table 5. Compiled Variance Results for Eight Full Stokes Polarimeter Configurations, under IG Noise[a]

Configuration	var($\hat{s}_0$)	var($\hat{s}_1$)	var($\hat{s}_2$)	var($\hat{s}_3$)	EWV	κ_1	κ_2	κ_∞	κ_F
Ambirajan-RRFP	2.00	7.25	10.67	1.72	21.64	8.33	3.52	5.89	6.58
Sabatke-RRFP	1.00	2.99	2.99	3.02	10.00	6.03	1.73	4.64	4.47
Tyo-DVRFP	1.00	3.01	2.99	3.01	10.01	5.64	1.73	4.19	4.47
Zallat-DRRFP	1.00	2.93	3.05	3.02	10.00	6.19	1.75	4.73	4.47
Shibata-RRPC	2.00	8.00	8.00	4.00	22.00	5.00	2.00	2.00	4.69
Iniesta-4	1.00	3.00	3.00	3.00	10.00	6.20	1.73	4.73	4.47
Iniesta-6	1.50	4.50	4.50	4.50	15.00	4.00	1.73	2.00	4.47
Azzam*	2.26	5.63	16.69	9.93	34.51	26.00	9.59	25.15	16.18
Kudenov-I*	1.34	7.00	34.07	221.41	263.82	81.14	14.91	74.00	48.49
Kudenov-II*	0.36	2.49	0.75	1.23	4.82	8.92	4.15	11.29	6.67

[a]All entries are in units of v_d/ϵ^2. Matrix condition numbers are provided for comparison. The starred configurations indicate that the tabulated results use the normalized photometric models.

satisfies independence of measurements and has a finite variance.

We can also see that both Azzam's four-detector polarimeter and the stacked photovoltaic polarimeter have higher variances, with particular difficulty detecting s_2 and s_3. However, if the optimized version of Kudenov's stacked-detector system can be implemented, we can see that its performance surpasses all of the other systems by a wide margin due to its efficient use of the input light.

From the condition numbers listed in Table 5, we can note that the 2-norm and Frobenius-norm condition numbers give the same result for every optimized system, whereas the 1-norm and infinity-norm condition numbers are more erratic, showing preference for one system over another even though the covariance metric shows that the performance is unchanged. Thus, if any condition number is to be used as a metric, then the former pair is to be preferred over the latter.

In addition, it is useful to note that despite the effort we took to efficiency normalize the Azzam and Kudenov systems, the condition numbers for these are unchanged because any definition for $\kappa(\mathbf{W})$ is invariant to a scalar factor in $\mathbf{W}$. Looking at the form of the covariance matrices, we can go even further and say that the appearance of ϵ as a scalar factor applied to $\mathbf{K}$ in the IG and PP noise regimes more or less justifies the past use of the condition number as a proxy for system performance. This works well in the limits of IG and PP noise but holds only approximately in the intermediate mixed PG noise regime.

Table 6. Compiled SNR Results for Eight Full Stokes Polarimeter Configurations, under IG Noise[a]

Configuration	SNR($\hat{s}_0$)	SNR($\hat{s}_1$)	SNR($\hat{s}_2$)	SNR($\hat{s}_3$)
	IG regime: $\square\ \epsilon/\sigma_d$)			
Ambirajan-RRFP	$0.71s_0$	$0.37s_1$	$0.31s_2$	$0.76s_3$
Sabatke-RRFP	$1.00s_0$	$0.58s_1$	$0.58s_2$	$0.58s_3$
Tyo-DVRFP	$1.00s_0$	$0.58s_1$	$0.58s_2$	$0.58s_3$
Zallat-DRRFP	$1.00s_0$	$0.58s_1$	$0.57s_2$	$0.57s_3$
Shibata-RRPC	$0.71s_0$	$0.35s_1$	$0.35s_2$	$0.50s_3$
Iniesta-4	$1.00s_0$	$0.58s_1$	$0.58s_2$	$0.58s_3$
Iniesta-6	$0.82s_0$	$0.47s_1$	$0.47s_2$	$0.47s_3$
Azzam*	$0.67s_0$	$0.42s_1$	$0.24s_2$	$0.32s_3$
Kudenov-I*	$0.86s_0$	$0.38s_1$	$0.17s_2$	$0.07s_3$
Kudenov-II*	$1.67s_0$	$0.63s_1$	$1.15s_2$	$0.91s_3$

[a]"□" indicates a table entry.

From the tabulated variances, Table 6 shows the corresponding SNRs of each system analyzed in the IG regime. As we expect from the variances listed in Table 5, we see that the idealized stacked detector has the highest performance. Its four SNR values (1.67, 0.63, 1.115, and 0.91) look somewhat close to (1.5, 1, 1, and 1), suggesting a possible limit for the "perfect polarimeter" when the input measurement light is given as $4s_0$.

9. CONCLUSIONS

Although recent research has shown how the variances of the Stokes parameters depend on the input SOP in PP noise, and that the variance behavior is generally different in the IG and PP noise regimes, several important features have gone unnoticed. In both the linear and the full Stokes polarimeters, we see that optimized designs exhibit the same covariance matrix structure, either 1:2:2 (for linear Stokes) or 1:3:3:3 (for full Stokes) ratios of variances, in both IG and PP noise regimes. This justifies the use of the simpler IG noise regime for calculating polarimeter optimization and to an extent also exonerates the use of matrix condition numbers for a proxy of system performance. Any system optimized under IG noise will be "equivariant" under PP noise. We can also note that no polarimeter design is able to diagonalize the covariance matrix under PP noise, so that even the idealized systems exhibit correlated noise characteristics.

Goudail has shown that, for PP noise, the maximum-likelihood estimator (MLE) can provide a significant boost in performance over the least squares estimators that we have used throughout the preceding analysis [28]. However, only those users who operate at very low light levels will be able to take advantage of this because the MLE provides better performance only when the number of measured photoelectrons ϵI is small (e.g., less than 10)—a level below which the Gaussian distribution can no longer be used as a good approximation to the Poisson or the PG mixed distribution.

An unexpected result in the exploration of linear Stokes polarimeter designs was the unique behavior of the optimized 0-60-120 configuration, in which the parameter variances depend on the amplitude of $\tilde{s}_1$ but not of $\tilde{s}_2$. All other optimized linear configurations—the 0-45-90-135 and any other setups that evenly sample the half-circle of angles—exhibit no dependence on the input SOP.

The incorporation of a photometric measurement model provides a foundation for building a mixed PG noise model and also enables the quantitative comparison of unusual systems, such as Azzam's four-detector polarimeter and Kudenov's stacked photovoltaic polarimeter, with more common instruments, such as the RRFP. The variance results indicate that the diattenuating designs so far have a lower performance, but they also have a lot of room for improvement, and so this is not an indication of any fundamental gap between the techniques. See the Code 1, Ref. [29] (written in ScientificPython) used for the covariance matrix calculations in the paper.

APPENDIX A: COVARIANCE MATRICES UNDER MIXED PG NOISE

Tables 7–14 give the full PG noise model covariance matrices for the full Stokes polarimeter systems compared. Each covariance matrix has been formatted into a table for readability, with

Table 7. PG Covariance Matrix for Ambirajan's RRFP Polarimeter

$K_{ij} =$	$\square s_0/\epsilon$	$+\square s_1/\epsilon$	$+\square s_2/\epsilon$	$+\square s_3/\epsilon$	$+\square v_d/\epsilon^2$
$K_{00} =$	1.01	0.14		0.24	2.01
$K_{01} =$	−1.31	−0.45		−0.24	−2.63
$K_{02} =$			0.62		
$K_{03} =$	0.07	−0.14		0.83	0.13
$K_{10} =$	−1.31	−0.45		−0.24	−2.63
$K_{11} =$	3.62	2.76		0.24	7.25
$K_{12} =$			−0.62		
$K_{13} =$	0.24	0.45		−0.83	0.49
$K_{20} =$			0.62		
$K_{21} =$			−0.62		
$K_{22} =$	5.33	1.33		−4.62	10.67
$K_{23} =$			−0.62		
$K_{30} =$	0.07	−0.14		0.83	0.13
$K_{31} =$	0.24	0.45		−0.83	0.49
$K_{32} =$			−0.62		
$K_{33} =$	0.86	0.14		0.10	1.72

Table 8. PG Covariance Matrix for Sabatke's RRFP Polarimeter

$K_{ij} =$	$\square s_0/\epsilon$	$+\square s_1/\epsilon$	$+\square s_2/\epsilon$	$+\square s_3/\epsilon$	$+\square v_d/\epsilon^2$
$K_{00} =$	0.50				1.00
$K_{01} =$		0.50			
$K_{02} =$			0.50		
$K_{03} =$				0.50	
$K_{10} =$		0.50			
$K_{11} =$	1.50				3.00
$K_{12} =$			0.50	−0.71	
$K_{13} =$			−0.71	−0.50	
$K_{20} =$			0.50		
$K_{21} =$			0.50	−0.71	
$K_{22} =$	1.50	0.50			3.00
$K_{23} =$		−0.71			
$K_{30} =$				0.50	
$K_{31} =$			−0.71	−0.50	
$K_{32} =$		−0.71			
$K_{33} =$	1.50	−0.50			3.00

Table 9. PG Covariance Matrix for Tyo's DVRFP Polarimeter

$K_{ij} =$	$\square s_0/\epsilon$	$+\square s_1/\epsilon$	$+\square s_2/\epsilon$	$+\square s_3/\epsilon$	$+\square v_d/\epsilon^2$
$K_{00} =$	0.50				1.00
$K_{01} =$		0.50			
$K_{02} =$			0.50		—
$K_{03} =$				0.50	0.01
$K_{10} =$		0.50			
$K_{11} =$	1.50	0.73		−0.59	3.01
$K_{12} =$			−0.27		0.01
$K_{13} =$		−0.58		−0.46	0.01
$K_{20} =$			0.50		
$K_{21} =$			−0.27		0.01
$K_{22} =$	1.49	−0.27	−0.01	0.82	2.99
$K_{23} =$			0.82	0.01	0.01
$K_{30} =$				0.50	0.01
$K_{31} =$		−0.58		−0.46	0.01
$K_{32} =$			0.82	0.01	0.01
$K_{33} =$	1.50	−0.46	0.01	−0.24	3.01

Table 10. PG Covariance Matrix for Zallat's DRRFP Polarimeter

$K_{ij} =$	$\square s_0/\epsilon$	$+\square s_1/\epsilon$	$+\square s_2/\epsilon$	$+\square s_3/\epsilon$	$+\square v_d/\epsilon^2$
$K_{00} =$	0.50				1.00
$K_{01} =$	−0.01	0.50			−0.03
$K_{02} =$			0.50	−0.01	
$K_{03} =$			−0.01	0.50	
$K_{10} =$	−0.01	0.50			−0.03
$K_{11} =$	1.47	0.01			2.93
$K_{12} =$			−0.20	0.84	
$K_{13} =$			0.83	0.20	
$K_{20} =$			0.50	−0.01	
$K_{21} =$			−0.20	0.84	
$K_{22} =$	1.53	−0.18			3.05
$K_{23} =$	0.03	0.86			0.05
$K_{30} =$			−0.01	0.50	
$K_{31} =$			0.83	0.20	
$K_{32} =$	0.03	0.86			0.05
$K_{33} =$	1.51	0.23			3.02

Table 11. PG Covariance Matrix for Iniesta's Four-Measurement Idealized Polarimeter

$K_{ij} =$	$\square s_0/\epsilon$	$+\square s_1/\epsilon$	$+\square s_2/\epsilon$	$+\square s_3/\epsilon$	$+\square v_d/\epsilon^2$
$K_{00} =$	0.50				1.00
$K_{01} =$		0.50			
$K_{02} =$			0.50		
$K_{03} =$				0.50	
$K_{10} =$		0.50			
$K_{11} =$	1.50				3.00
$K_{12} =$				0.87	
$K_{13} =$			0.87		
$K_{20} =$			0.50		
$K_{21} =$				0.87	
$K_{22} =$	1.50				3.00
$K_{23} =$		0.87			
$K_{30} =$				0.50	
$K_{31} =$			0.87		
$K_{32} =$		0.87			
$K_{33} =$	1.50				3.00

Table 12. PG Covariance Matrix K* for Azzam's Four-Detector Polarimeter

$K_{ij} =$	$\square s_0$	$+\square s_1$	$+\square s_2$	$+\square s_3$	$+\square v_d$
$K_{00} =$	1.07	0.19	−0.09		2.26
$K_{01} =$	1.53	0.33	−0.15	−0.03	3.37
$K_{02} =$	−1.02	−0.55	0.25	−0.06	−2.64
$K_{03} =$	0.27	0.05	−0.03	0.16	0.26
$K_{10} =$	1.53	0.33	−0.15	−0.03	3.37
$K_{11} =$	3.05	−0.01	−0.26	−0.15	5.63
$K_{12} =$	−0.77	−1.51	0.11	−0.60	−3.12
$K_{13} =$	−0.27	0.34	−0.21	0.30	−0.50
$K_{20} =$	−1.02	−0.55	0.25	−0.06	−2.64
$K_{21} =$	−0.77	−1.51	0.11	−0.60	−3.12
$K_{22} =$	11.24	−4.11	0.68	−2.05	16.69
$K_{23} =$	−2.38	0.30	−0.37	2.42	−8.41
$K_{30} =$	0.27	0.05	−0.03	0.16	0.26
$K_{31} =$	−0.27	0.34	−0.21	0.30	−0.50
$K_{32} =$	−2.38	0.30	−0.37	2.42	−8.41
$K_{33} =$	4.98	−1.84	0.97	−2.09	9.93

Table 13. PG Covariance Matrix K* for the Kudenov-I Stacked Photovoltaic Polarimeter

$K_{ij} =$	$\square s_0$	$+\square s_1$	$+\square s_2$	$+\square s_3$	$+\square v_d$
$K_{00} =$	0.36	0.11		−0.03	1.34
$K_{01} =$	0.41	0.43		−0.08	2.89
$K_{02} =$	−0.23	−0.15	0.31	0.08	−1.42
$K_{03} =$	−1.59	−1.19	0.06	0.74	−13.87
$K_{10} =$	0.41	0.43		−0.08	2.89
$K_{11} =$	2.01	0.49		−0.18	7.00
$K_{12} =$	−0.79	−0.21	0.71	0.19	−3.35
$K_{13} =$	−2.47	−3.21	0.13	1.68	−31.10
$K_{20} =$	−0.23	−0.15	0.31	0.08	−1.42
$K_{21} =$	−0.79	−0.21	0.71	0.19	−3.35
$K_{22} =$	12.90	4.84	3.02	0.86	34.07
$K_{23} =$	5.12	4.53	2.49	−1.68	42.67
$K_{30} =$	−1.59	−1.19	0.06	0.74	−13.87
$K_{31} =$	−2.47	−3.21	0.13	1.68	−31.10
$K_{32} =$	5.12	4.53	2.49	−1.68	42.67
$K_{33} =$	41.42	23.11	−0.86	−7.29	221.41

Table 14. PG Covariance Matrix $[K_{II}^*]$ for the Kudenov-II Stacked Photovoltaic Polarimeter

$K_{ij} =$	$\square s_0$	$+\square s_1$	$+\square s_2$	$+\square s_3$	$+\square v_d$
$K_{00} =$	0.34	0.01	0.14		0.36
$K_{01} =$	−0.32	0.14	−0.17	−0.04	−0.31
$K_{02} =$	0.26	0.04	0.38	0.03	0.29
$K_{03} =$	0.03		0.06	0.15	0.06
$K_{10} =$	−0.32	0.14	−0.17	−0.04	−0.31
$K_{11} =$	2.43	0.16	−0.76	0.18	2.49
$K_{12} =$	−0.87	−0.30	−0.46	−0.11	−0.98
$K_{13} =$	−0.19	0.06	−0.16	0.80	−0.06
$K_{20} =$	0.26	0.04	0.38	0.03	0.29
$K_{21} =$	−0.87	−0.30	−0.46	−0.11	−0.98
$K_{22} =$	0.70	0.10	0.36	0.07	0.75
$K_{23} =$	0.09	−0.01	0.15	−0.27	0.05
$K_{30} =$	0.03		0.06	0.15	0.06
$K_{31} =$	−0.19	0.06	−0.16	0.80	−0.06
$K_{32} =$	0.09	−0.01	0.15	−0.27	0.05
$K_{33} =$	1.17	0.40	−0.35	−0.09	1.23

each row listing a matrix entry. In addition, factors shared by every element in a column are listed at the top of the column, and entries whose value is zero are left blank. Thus, a table header and an entry row listed as

$$\begin{array}{lccccc} K_{ij} = & \square s_0/\epsilon & +\square s_1/\epsilon & +\square s_2/\epsilon & +\square s_3/\epsilon & +\square v_d/\epsilon^2 \\ K_{00} = & 1.01 & 0.14 & & -0.24 & 2.01 \end{array}$$

means that the K_{00} entry is written out in full equation form as

$$K_{00} = 1.01\frac{s_0}{\epsilon} + 0.14\frac{s_1}{\epsilon} + 0\frac{s_2}{\epsilon} - 0.24\frac{s_3}{\epsilon} + \frac{2.01}{\epsilon^2}v_d.$$

Funding. Japan Society for the Promotion of Science (JSPS) (15H03941).

Acknowledgment. The authors thank Ruonan Yang and Michael Kudenov for helpful comments on the paper.

REFERENCES

1. D. S. Sabatke, M. R. Descour, E. L. Dereniak, W. C. Sweatt, and S. A. Kemme, "Optimization of retardance for a complete Stokes polarimeter," Opt. Lett. **25**, 802–804 (2000).
2. J. S. Tyo, "Noise equalization in Stokes parameter images obtained by use of variable-retardance polarimeters," Opt. Lett. **25**, 1198–1200 (2000).
3. J. S. Tyo, "Design of optimal polarimeters: Maximization of signal-to-noise ratio and minimization of systematic error," Appl. Opt. **41**, 619–630 (2002).
4. I. J. Vaughn and B. G. Hoover, "Noise reduction in a laser polarimeter based on discrete waveplate rotations," Opt. Express **16**, 2091–2108 (2008).
5. J. S. Tyo, D. L. Goldstein, D. B. Chenault, and J. A. Shaw, "Review of passive imaging polarimetry for remote sensing applications," Appl. Opt. **45**, 5453–5469 (2006).
6. R. A. Chipman, "Polarimetry," in *Handbook of Optics*, M. Bass, ed. (McGraw-Hill, 1995), Vol. 2, Chap. 22.
7. O. S. Dron, "Random errors and optimum estimation of measurements photometric ellipsometers," Phys. Status Solidi **5**, 1068–1072 (2008).
8. D. L. Snyder, C. W. Helstrom, A. D. Lanterman, M. Faisal, and R. L. White, "Compensation for readout noise in CCD images," J. Opt. Soc. Am. A **12**, 272–283 (1995).
9. H. H. Barrett, C. Dainty, and D. Lara, "Maximum-likelihood methods in wavefront sensing: stochastic models and likelihood functions," J. Opt. Soc. Am. A **24**, 391–414 (2007).
10. F. Goudail, "Noise minimization and equalization for Stokes polarimeters in the presence of signal-dependent Poisson shot noise," Opt. Lett. **34**, 647–649 (2009).
11. G. D. Bernard and R. Wehner, "Functional similarities between polarization vision and color vision," Vis. Res. **17**, 1019–1028 (1977).
12. J. S. Tyo, "Optimum linear combination strategy for an N-channel polarization-sensitive imaging or vision system," J. Opt. Soc. Am. A **15**, 359–366 (1998).
13. R. Perkins and V. Gruev, "Signal-to-noise analysis of Stokes parameters in division of focal plane polarimeters," Opt. Express **18**, 25815–25824 (2010).
14. A. Peinado, A. Lizana, J. Vidal, C. Iemmi, and J. Campos, "Optimization and performance criteria of a Stokes polarimeter based on two variable retarders," Opt. Express **18**, 9815–9830 (2010).
15. A. Ambirajan and D. C. Look, Jr., "Optimum angles for a polarimeter: Part I," Opt. Eng. **34**, 1651–1655 (1995).
16. J. Zallat, S. Aïnouz, and M. P. Stoll, "Optimal configurations for imaging polarimeters: impact of image noise and systematic errors," J. Opt. A **8**, 807–814 (2006).
17. R. M. A. Azzam, "Arrangement of four photodetectors for measuring the state of polarization of light," Opt. Lett. **10**, 309–311 (1985).

18. R. Yang, P. Sen, B. T. O'Connor, and M. W. Kudenov, "Intrinsic coincident full-Stokes polarimeter using stacked organic photovoltaics," Appl. Opt. **56**, 1768–1774 (2017).
19. S. Shibata, T. Onuma, and Y. Otani, "Real-time birefringence mapping by full-Stokes polarization camera," in *6th International Conference on Spectroscopic Ellipsometry (ICSE VI)*, 2013.
20. J. S. Tyo, "Relation between system optimization and systematic errors in Stokes vector polarimeters," Proc. SPIE **4481**, 22–30 (2002).
21. A. D. Martino, Y.-K. Kim, E. Garcia-Caurel, B. Laude, and B. Drévillon, "Optimized Mueller polarimeter with liquid crystals," Opt. Lett. **28**, 616–618 (2003).
22. J. C. del Toro Iniesta and M. Collados, "Optimum modulation and demodulation matrices for solar polarimetry," Appl. Opt. **39**, 1637–1642 (2000).
23. T. Mu, Z. Chen, C. Zhang, and R. Liang, "Optimal configurations of full-Stokes polarimeter with immunity to both Poisson and Gaussian noise," J. Opt. **18**, 055702 (2016).
24. B. H. Miles, R. A. Goodson, E. L. Dereniak, and M. R. Descour, "Computed-tomography imaging spectropolarimeter (CTISP): instrument concept, calibration and results," Proc. SPIE **3754**, 235–245 (1999).
25. S. G. Roy, O. M. Awartani, P. Sen, B. T. O'Connor, and M. W. Kudenov, "Intrinsic coincident linear polarimetry using stacked organic photovoltaics," Opt. Express **24**, 14737–14747 (2016).
26. R. M. A. Azzam, "Instrument matrix of the four-detector photopolarimeter: physical meaning of its rows and columns and constraints on its elements," J. Opt. Soc. Am. A **7**, 87–91 (1990).
27. M. Kudenov, (2017, personal communication).
28. F. Goudail, "Performance comparison of pseudo-inverse and maximum-likelihood estimators of Stokes parameters in the presence of Poisson noise for spherical design-based measurement structures," Opt. Lett. **42**, 1899–1902 (2017).
29. Python code for covariance matrix calculations, figshare https://doi.org/10.6084/m9.figshare.6163874.

applied optics

Stokes polarimeter performance: general noise model and analysis: erratum

Nathan Hagen,[1,*] Tingkui Mu,[2] and Yukitoshi Otani[1]

[1]Utsunomiya University, Department of Optical Engineering, Center for Optical Research and Engineering (CORE), 7-1-2 Yoto, Utsunomiya, Tochigi 321-0954, Japan
[2]Institute of Space Optics (ISO), Department of Opto-Electronics Information Science and Engineering, School of Science, Xi'an Jiaotong University, Xi'an Shaanxi 710049, China
*Corresponding author: nh@hagenlab.org

Received 13 July 2018; posted 21 July 2018 (Doc. ID 338738); published 17 August 2018

We correct two errors in Appl. Opt. 57, 4283 (2018).

OCIS codes: (260.5430) Polarization; (280.0280) Remote sensing and sensors; (230.5440) Polarization-selective devices; (030.4280) Noise in imaging systems.

https://doi.org/10.1364/AO.57.006998

On page 4285 of the original paper [1], the unnumbered equation appearing immediately before the numbered Eq. (5) was given incorrectly. The covariance matrix should be diagonal, i.e.,

$$\mathbf{K}_{\mathrm{IG}} = \begin{pmatrix} \mathrm{var}(\hat{s}_0) & \mathrm{cov}(\hat{s}_0,\hat{s}_1) & \mathrm{cov}(\hat{s}_0,\hat{s}_2) \\ \mathrm{cov}(\hat{s}_1,\hat{s}_0) & \mathrm{var}(\hat{s}_1) & \mathrm{cov}(\hat{s}_1,\hat{s}_2) \\ \mathrm{cov}(\hat{s}_2,\hat{s}_0) & \mathrm{cov}(\hat{s}_2,\hat{s}_1) & \mathrm{var}(\hat{s}_2) \end{pmatrix} = \frac{v_{\mathrm{d}}}{\epsilon^2}\begin{pmatrix} 1 & 0 & 0 \\ 0 & 2 & 0 \\ 0 & 0 & 2 \end{pmatrix}.$$

In addition, for Sabatke's RRFP, the covariance matrix in the PP noise limit given in Section 4.B (page 4289) of the original paper is not correct. Two terms are missing from the diagonal, so that the result should be

$$\mathbf{K}_{\mathrm{PP}} = \frac{s_0}{2\epsilon}\begin{pmatrix} 1 & \tilde{s}_1 & \tilde{s}_2 & \tilde{s}_3 \\ \tilde{s}_1 & 3 & \tilde{s}_2 - \sqrt{2}\tilde{s}_3 & -\sqrt{2}\tilde{s}_2 - \tilde{s}_3 \\ \tilde{s}_2 & \tilde{s}_2 - \sqrt{2}\tilde{s}_3 & 3 + \tilde{s}_1 & -\sqrt{2}\tilde{s}_1 \\ \tilde{s}_3 & -\sqrt{2}\tilde{s}_2 & -\sqrt{2}\tilde{s}_1 & 3 - \tilde{s}_1 \end{pmatrix}.$$

This change affects one of the assertions given in the Conclusion, where it is stated that "Any system optimized under IG noise will be "equivariant" under PP noise." The corrected form of the matrix is obviously not equivariant. Likewise, the covariance matrices for Tyo's DVRFP and Zallat's DRRFP polarimeter (Tables 9 and 10 on page 4294) demonstrate that these systems will not be equivariant as well. Thus, this assertion is incorrect.

The remainder of the paper is unaffected, and these changes do not affect the code provided with the paper for calculating the covariance matrices.

REFERENCE

1. N. Hagen and Y. Otani, "Stokes polarimeter performance: general noise model and analysis," Appl. Opt. **57**, 4283–4296 (2018).